Specular color imaging on a metallic substrate

Petar Pjanic, Roger D. Hersch; School of Computer and Communication Sciences, Ecole Polytechnique Fédérale de Lausanne (EPFL), Lausanne, Switzerland

Abstract

We propose a full reproduction workflow for printing color images on metallic substrates. It relies on an ink spreading enhanced cellular Yule-Nielsen modified spectral Neugebauer model, calibrated with 35 color samples printed on the metal film and measured under specular reflection. The calibration accounts for the different phenomena contributing to the reflectance of halftone prints on metal: specular reflection by the metal film substrate of light traveling across the inks, illumination and viewing geometry, shadowing effect induced by the ink and difference in surface structure between the inked and non-inked metal halftone elements. The model enables predicting printable colors with an average CIELAB ΔE_{94} error of 1.7. Thanks to the model, the metal print gamut is established and a 3D table provides the correspondence between printable metallic colors viewed under specular reflection and the corresponding ink surface coverages. The input sRGB gamut is mapped into the print gamut. At halftone image generation time, surface coverages of the inks yielding the desired gamut mapped input colors are obtained from the 3D table. These ink surface coverages yield the ink separations that are halftoned and printed. The resulting color images printed on a silver substrate viewed under specular reflection reproduce the hues at a high degree of fidelity. The luminance of metallic prints under specular observation is generally higher than the luminance of paper under the same illuminating conditions. Therefore, the printed metallic colors appear more colorful. Such metal prints are attractive for design, art and publicity. Their high brightness immediately strikes the observer and transmits the message incorporated into the reproduced picture or artwork.

Introduction

Metal substrates are increasingly used in the packaging industry. Packaging design has the primary goal to attract the customers' attention by communicating emotions. At present, most of today's package illustrations are made by printing color designs and motives on a diffuse white layer located on top of the metallic substrate. Direct printing on a metallic substrate however would create color prints, which, when viewed under specular reflection provide bright and brilliant colors. Our aim is to present a color reproduction workflow specially tailored for printing color images on metallic substrates to be viewed under specular reflection.

Classical color reproduction workflows [1] rely on the characterization of the target printing device, on the establishment of the target printer gamut, on the mapping of the input color gamut, e.g. the display sRGB gamut, onto the target printer gamut, on the establishment of a correspondence table between desired gamut mapped output color and ink dot surface coverages and on the halftoning and printing of the ink layers (Figure 1).

Printing color images on a highly specular substrate such as a silver based film layer [2] raises several challenges. A first set of challenges relates to colorimetric and appearance prediction models. Colorimetric systems such as CIE-XYZ, color appearance models such as CIECAM02 and image appearance models [3] were established under diffuse lighting conditions and for diffusely emitting or reflecting media. A recent study also considered the perceived lightness of luminescence values that are higher than the ones diffusely reflected by a paper surface [4]. However, to our knowledge, no attempts have been made to validate color appearance models under specular reflection from a metallic surface.

Color and image appearance models such as CIECAM02 [5] [6] account for the adaptation of the human visual system to the background, the surround and the brightest part of the visual field. These models were built by having observers viewing a target sample incorporating a white reflective patch acting as reference white, surrounded by a neutral background. In the case of a color picture printed on a metallic surface that is illuminated by directed light, e.g. by light from a window, it is not clear how the eye adapts to the specularly reflecting metallic image [7].

A second set of challenges relates to the physics of the print and its interaction with light. Since ink printed on the metal layer slightly scatters the ink, the angular distribution of reflected light from ink on metal is not the same as the one from the bare metal film. In addition, the ink has a certain thickness, and ink halftones printed on metal illuminated by directed light project their shadows on the blank metallic surface between ink dots, thereby reducing the effective size of their specularly reflecting surface.

In the present work, we propose a color reproduction workflow for printing color images on a metallic surface. This reproduction workflow uses CIELAB as a color space for establishing the print gamut and for gamut mapping. The proposed color reproduction workflow enables producing metallic color images that are to be viewed under specular viewing conditions.

Related work and background

The prior work spans different research areas. In the field of printing, Dalal and Natale-Hoffman [8] modeled the reflectance of glossy xerographic paper prints under different observation angles. When measured or observed at non specular angles, a glossy print considerably increases the saturation of images since the lightness component due to specular reflection is discarded. Mikula et al. [9] analyzed the effect of gloss on the reflectance of an ink printed on a given substrate, such as varnished paper, non-varnished paper and aluminium, in function of the detection angle. At specular angles, on a metallized substrate, they observed strong increases in lightness and in chroma and as well as hue shifts when moving

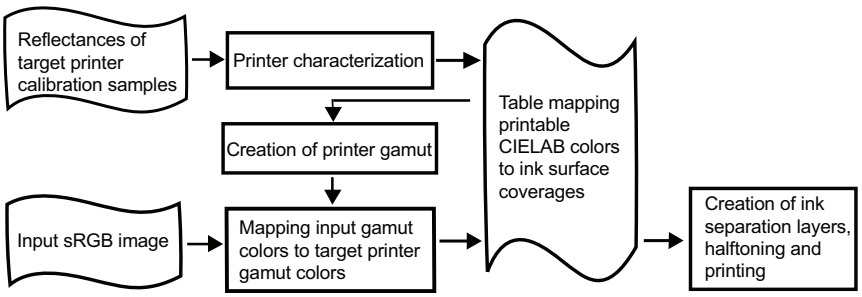

***Figure 1**. A classical color reproduction workflow*

from non-specular to specular capture angles. Hersch et al. [10] created a new security feature by combining metallic ink and standard inks to print color images with embedded metallic color patterns. These patterns are hidden when observed under non-specular observation angles and revealed under specular observation angles. Matusik et al. [11] extended classical color reproduction with the aim of reproducing also the BRDF of a flat original. For this purpose, they used a blend of standard inks and of glossy metallic inks with specific BRDF's and reproduced the original by an extended halftoning process.

In respect to models predicting the color of a print as a function of the dot surface coverages of the contributing inks, the most widely used spectral prediction model is the Yule-Nielsen modified Spectral Neugebauer model [12], [13]. This model has been further improved by subdivision of the ink surface coverage space [14] and by accounting for ink spreading within each subspace. This yields for prints on paper very accurate predictions [15].

In the field of colorimetry, there is no standard system for characterizing the reflected metallic colors. Simonot et. al. [16] extrapolated the CIELAB system to specular samples. Since their reference is the perfect white Lambertian diffuser, they obtain for the specular reflectance of a perfect mirror, captured at a detector half-angle of 10° a lightness L^*=357. These extrapolated CIELAB values may be useful for specific tasks such as exploration of gamut volumes, creation of color histograms or color segmentation. However, their applicability for expressing perceptually correct color differences is uncertain [4].

In respect to color appearance models, Johnson and Fairchild [17] provide an excellent overview. The book by Fairchild [3] describes in detail the psychophysical experiments on which the different color appearance models are built. Relevant for the present work are *chromatic adaptation*, as suggested by von Kries and formulated by Hunt and Pointer [18], which adjusts the perception of colors to the color and intensity of the overall illumination. Also relevant is the *Hunt effect* [19] which states that when the luminance of a given color increases its perceived colorfulness also increases. The *Stevens effect* [20] states that as the luminance level increases, so does also the brightness contrast. Scenes appear more contrasted when viewed in a bright environment. *The Helmholtz-Kohlrausch effect* states that a chromatic stimulus appears brighter than an achromatic stimulus at the same luminance [21].

The reflectance of specularly observed ink halftones on metal

In the present work, we consider ink halftones printed on a flat metallic surface. We assume that the halftone print on metal is viewed under light from a window or from a light table. Since the ink is either non-diffusing or very little diffusing, the observed halftones are viewed under specular reflection (Figure 2a). We have created a similar but not identical reflectance measurement setup where, due to the specular nature of the reflectance, the illumination and observation angles are equal, centered on the (25°:25°) geometry and where the capturing light cone (half-angle: 12.5°) is inside the illuminated surface (Figure 2b).

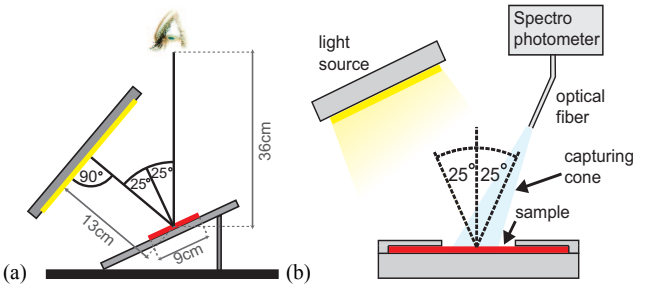

***Figure 2**. (a) Specular observation of a metallic print illuminated by a light table and (b) optical setup for capturing the specular reflectance factor of a metallic print sample. Both the light table and the light source emit position-independent diffuse white light.*

Halftones printed on metal have a certain elevation over the metallic surface. When illuminated by directed light, such as the light coming from a window, depending on the illumination angle and on the observation angle, a "shadowing" effect seems to appear (Figure 3).

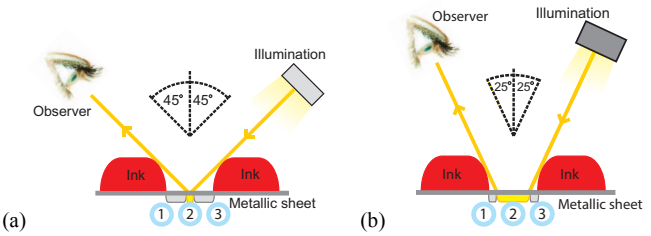

***Figure 3**. A shadowing effect may reduce the reflective surface part (2) of the blank metal as a function of the observation angle.*

This "shadowing" effect is more or less pronounced depending on the halftone screen surface coverage, screen frequency and the observation angle. The graph in Figure 4 shows the specularly reflected CIELAB lightness of black halftones printed on metal at 25%, 50%, 75% and 100% surface coverages, for capturing angles of 15°, 25°, 35°, and 45°, at a screen frequency of 100 lpi. The reference white for the CIELAB lightness computation is the CIE-YXZ tri-stimulus value of the unprinted metal film substrate in specular reflection measured under the same specular angle as the test sample. Information concerning the printer and the substrate are given in the section "Test of the model…".

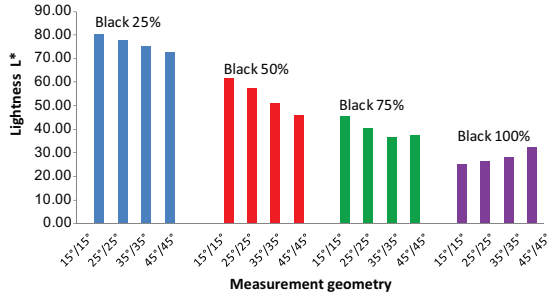

***Figure 4**. Lightnesses (CIELAB L*) of a black halftone printed on a metallic sheet*

Fig. 4 shows that the strongest decrease in lightness with increasing measurement angles occurs at a halftone of 50% surface coverage. At that surface coverage, the boundary between ink surface and metal surface is the largest and the shadowing effect has the strongest effect. The lightness of L^*=61.5 at 15° decreases to a lightness of L^*=46.2 at 45°. At 100% surface coverage of black, there is no shadowing effect since the full tone already covers all metal film areas. A small inverse effect appears, i.e. towards 45°, the specularly reflected lightness becomes stronger.

The color reproduction workflow adapted to metallic prints

A classical color reproduction workflow comprises the steps of (a) characterization of the target printer by establishing a correspondence between ink surface coverages and resulting printed color, (b) establishing the color gamut of the target printing device by computing the not necessarily convex hull of all possible printed colors, (c) performing gamut mapping between the input gamut, e.g. the sRGB display gamut and the target printing gamut, (d) color separating the gamut mapped colors into individual ink layers by making use of the correspondence between desired printed color and ink surface coverages and (e) halftoning and printing the individual ink layers.

Gamut mapping ensures that all the considered display colors can be printed. For each display color there will be a combination of ink surface coverages that will produce the corresponding mapped color located within the print gamut.

In reproduction workflows for classical halftone prints on paper, the characterization of the target printer is performed either by a black box approach or by making use of a color prediction model. The black box approach consists in printing color patches of all combinations of inks at closely spaced dot surface coverages, e.g. 10%, 20%, ... 100% and in measuring the reflectance factor of each patch, converting it to a CIELAB color and populating a table creating the correspondence between desired output color and ink surface coverages.

In the present work, we are interested in creating a reproduction workflow for color images to be viewed under specular reflection. Therefore, our measurements must be performed under similar conditions as the viewing conditions, i.e. illumination by a large surface mimicking a window and observation at a preferred angle of 25°. For the characterization of the target printer, it would be tedious to follow the black box approach and to try to measure more than thousand samples in specular mode. We therefore made use of the cellular Yule-Nielsen modified spectral Neugebauer prediction model enhanced to account for ink spreading (IS-CYNSN), see [15].

The ink-spreading enhanced cellular Yule-Nielsen modified spectral Neugebauer prediction model (IS-CYNSN) enhanced to account for ink spreading

The IS-CYNSN reflectance prediction model relies on the same principles as the Yule-Nielsen modified Spectral Neugebauer (YNSN) model [1]. In the YNSN model, the predicted reflectance is

$$R(\lambda) = \left(\sum_i a_i R_i(\lambda)^{1/n} \right)^n \qquad (1)$$

where a_i is the effective surface coverage of the i^{th} *colorant* (also called Neugebauer primary), R_i is its reflection spectrum and n is an empirical scalar coefficient related to the halftone screen frequency and to the halftone dot profile ($1< n <100$). In the YNSN model, the colorants are formed by all variations of superposed solid inks, i.e. all variations of nominal surface coverages of 0 and 1. For the 3 inks cyan (c), magenta (m) and yellow (y), we obtain the 2^3=8 colorants white (a_w: no ink), cyan only (a_c), magenta (a_m), yellow (a_y), red (a_r: m & y), green (a_g: c & y), blue (a_b: c & m), black (a_k: c & m & y). In the case of the IS-CYNSN reflectance prediction model, the 3D c, m, y ink space is subdivided into 8 subcubes whose corners are given by colorants formed by superpositions of c, m, y nominal surface coverages of 0, 0.5 and 1, i.e. combinations of no ink, ink at 50% surface coverage and solid ink. For 3 inks, we obtain 3^3=27 colorants (primaries). One of the subcubes is shown in Figure 5.

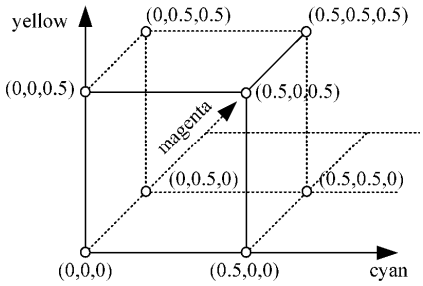

***Figure 5**. The subcube represents one of the 8 subcubes produced by the combinations of 0%, 50% and 100% surface coverages of the three inks. At the vertices (c,m,y) of the subcube, primary reflectances $R_{c,m,y}(\lambda)$ have been measured.*

Within each subcube, the normalized surface coverages $\hat{c}$, $\hat{m}$, $\hat{y}$, are given by

$$\hat{c} = \frac{c - c_l}{c_h - c_l} \qquad \hat{m} = \frac{m - m_l}{m_h - m_l} \qquad \hat{y} = \frac{y - y_l}{y_h - y_l} \tag{2}$$

where subcubes are delimited by $c \in [c_l,c_h]$, $m \in [m_l,m_h]$ and $y \in [y_l,y_h]$, In order to predict reflectances, the effective surface coverages a_i to be inserted into formula (1) are given by the Demichel equations

$$\begin{aligned} a_w &= (1-c')(1-m')(1-y') & a_c &= c'(1-m')(1-y') \\ a_m &= (1-c')m'(1-y') & a_y &= (1-c')(1-m')y' \\ a_r &= (1-c')m'y' & a_g &= c'(1-m')y' \\ a_b &= c'm'(1-y') & a_k &= c'm'y' \end{aligned} \tag{3}$$

Due to the spreading of ink dots on the underlying substrate and inks, the normalized effective surface coverages *c'*, *m'*, *y'* differ from the normalized nominal surface coverages $\hat{c}$, $\hat{m}$, $\hat{y}$, that the printer is asked to print. Figure 6 shows an ink spreading curve mapping normalized nominal ink surface coverages to normalized effective surface coverages $\hat{u} \rightarrow f(\hat{u})$.

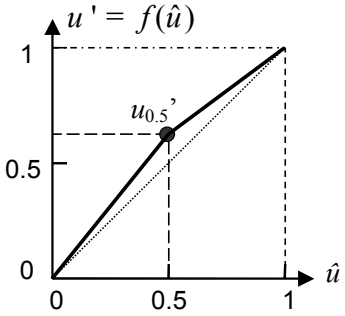

***Figure 6**. : Ink spreading curve mapping normalized nominal ink surface coverages $\hat{u}$ to normalized effective surface coverages u', where u' stands for c', m', or y'.*

We recover the ink spreading curves mapping normalized nominal to normalized effective dot sizes by printing the *cmy* color sample located at the center of each subcube, e.g. by printing nominal surface coverages of c=0.25, m=0.25, and y=0.25 for the first subcube defined by the ink surface coverage intervals $[c_l,c_h]$=[0,0.5], $[m_l,m_h]$=[0,0.5], $[y_l,y_h]$=[0,0.5]. Normalized effective dot sizes $c_{0.5}'$, $m_{0.5}'$, $y_{0.5}'$ at the center of each subcube are fitted by minimizing the square difference between the measured reflectance and the reflectance predicted by inserting Eqs. (3) into Eq. (1). Within each subcube, the three ink spreading curves mapping normalized nominal to normalized effective surface coverages are formed by linear interpolation between points (0,0), (0.5, $u_{0.5}'$), (1,1), where $u_{0.5}'$ is a place holder for the fitted normalized effective surface coverages of each ink $c_{0.5}'$, $m_{0.5}'$ and $y_{0.5}'$ at the center of each subcube.

Given the nominal ink surface coverages *c*, *m* and *y*, reflectances *R(c, m, y)* are predicted by locating the corresponding ink surface coverage subcube, by computing the normalized nominal ink surface coverages (Eqs. (2)), by obtaining thanks to the ink spreading curves the normalized effective ink surface coverages, by obtaining the effective colorant surfaces coverages thanks to the Demichel equations (3) and by inserting them into the YNSN equation (1).

For three inks, in addition to the 27 printed samples needed for the colorant reflectances at the vertices of the subcubes, we need 8 additional printed samples at the centers of the subcubes in order to derive for each subcube the 3 ink spreading curves. In total, with 35 measured reflectances for the calibration of the model, we can predict the reflectance and therefore the color of any printable set of ink surface coverages.

Note that in the case of specular measurements on a metallic substrate, instead of measuring, respectively predicting reflectances, we measure, respectively predict reflectance factors. They indicate, for the given illuminating and capturing geometries, how much a sample printed on the metallic substrate reflects in respect to the reflection of the unprinted metallic substrate.

The IS-CYNSN reflectance prediction model can be extended to predict colors by adding the formula calculating CIE-XYZ tri-stimulus values and then CIELAB values from predicted reflectance factors under a given illuminant, for the considered reference white. In the present case, the reference white is given by the CIE-XYZ values of the unprinted metal film substrate.

By comparing predicted and measured reflectance factors of 125 samples printed with *cmy* inks on the metal substrate at combinations of surface coverages 0, 0.25, 0.5, 0.75, 1, we obtain the prediction accuracy.

Test of the model predicting the specular reflectance factors of color halftone samples printed on the metal film

For all samples and images, we used the Epson Stylus Pro WT7900 printer at a resolution of 1440 dpi, with classical rotated clustered dots at a screen frequency of 100 lpi. Test samples and images are printed either on the metal film substrate, or for comparison purposes, on the double coated matt inkjet paper PRC 180HQ.

The samples are measured at specular illumination and reflection angles centered around 25°, as shown in the setup of Figure 2b. The light source is a 150W Halogen Dolan-Jenner DC-950H DC-Regulated Fiber Optic Illuminator connected through a fiber optic light guide to a 4.25"x 3.37" illuminator from Edmund Optics providing a highly diffuse and even light distribution. An optical fiber having a 600 µm diameter and a 12.5° half-angle cone aperture mounted on a graded rotational stage collects the light reflected from the sample at 25°. The optical fiber is connected to a Maya 2000 Pro back-thinned CCD spectrophotometer from Ocean Optics.

Reflectance factors are obtained by dividing the captured irradiance of the considered printed metal halftone sample by the captured irradiance of an unprinted metal sample. For calculating the CIE-XYZ tri-stimulus values, the specular reflection by the unprinted aluminum sample is the strongest and is therefore set to a Y value of 100. This same unprinted metal sample is also used as the reference white for the calculation of the CIELAB values of the color patches from their CIE-XYZ values [22, pp. 20-32].

The prediction accuracy achieved by the cellular ink spreading enhanced Yule-Nielsen model is given in Table I. Given the fact that reflectance factors are measured on an optical bench

Table I. IS-CYNSN model prediction error for 125 color samples, respectively 90 samples excluding the calibration samples, printed on a metallic film substrate, measured at a specular reflection angle of 25°, *n*-value is 14.

	Mean ΔE_{94}	95% quantile	max. ΔE_{94}	average rms
With calibration samples (125 samples)	1.26	3.88	5.75	0.007
Without calibration samples (90 test samples)	1.68	4.22	5.75	0.010

and that the irradiance reflected at specular angles is strongly dependent on the accuracy of the measurement setup (incident angle, capturing angle, capturing cone), the achieved prediction accuracy is remarkable.

Establishing the print gamut

In order to create a color reproduction workflow, we need first to establish the print gamut in a device-independent color space such as CIELAB. We then create a gamut mapping between the original sRGB display gamut and the print gamut. Gamut mapping ensures that all colors located within the original input gamut are reproducible on the target print. All measurements are carried out as described in the previous section.

The print gamut is established by predicting with the IS-CYNSN spectral prediction model the reflectance factors of halftones on the metal film substrate. We vary the nominal ink surface coverages in small steps for the three cyan, magenta and yellow inks, convert them to CIE-XYZ tri-stimulus values under the D65 illuminant and compute the corresponding CIELAB colors. The non-convex print gamut boundary is obtained by performing a Delaunay triangulation of the CIELAB color points and by computing with the Ball-Pivoting algorithm [23] the set of surface triangles forming the partly concave boundary (Figure 7, colored volume).

The sRGB input image gamut is obtained by varying the sRGB red, green and blue values in small steps, convert them first to CIE-XYZ values and then to CIELAB. We then establish the partly concave gamut by Delaunay triangulation and ball-pivoting [23]. The resulting gamut is displayed as a mesh grid in Figure 7.

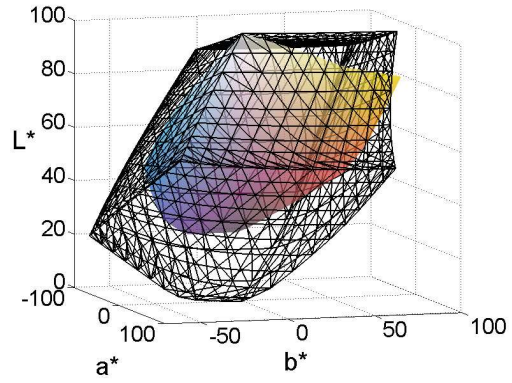

***Figure 7**. Respective gamuts of the sRGB display (mesh grid) and of the metallic color prints (color volume) under specular reflection, when setting the reference white to the color of the unprinted metallic film.*

When observed under specular reflection, the color prints on metal seem brighter and more colorful than the corresponding color prints on paper. However, as can be seen from Figure 8, the gamut of metal prints whose colors have been computed by assuming the blank metal film reflection as the "white" CIELAB reference is a little smaller than the gamut of paper.

This indicates that the eye possibly adapts to a lower level of intensity than the specular reflection of blank metal. By lowering the "white" reference CIE-XYZ tri-stimulus values by a constant multiplicative factor $0<g<=1$, we obtain $1/g^{1/3}$ larger CIELAB values (see Appendix). For example, by assuming as white reference the blank metal CIE-XYZ values scaled down by g=0.6, the corresponding metal color print gamut in CIELAB would increase by approximately a factor of 1.2 along each axis.

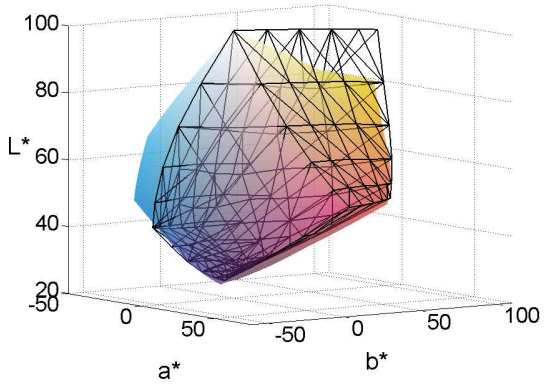

***Figure 8**. Comparison of the respective color gamuts of cmy prints on the PRC 180 HQ double coated matt inkjet paper (mesh) and on the metallic film substrate (color volume).*

However, thanks to gamut mapping, the relationship between original image colors (sRGB) and surface coverages of the inks in the target print does not strongly depend on the chosen adapting white reference. The reflectance factor of a given color print on metal depends of the nominal surface coverages of the inks that were used to print that sample. By performing the gamut mapping between the sRGB input gamut and the target print gamut in CIELAB space, we establish correspondences between sRGB values and ink surface coverage values. When the input gamut lightnesses are mapped linearly to the output gamut lightnesses and when, by keeping the lightness constant, the range of input chromaticities is mapped hue angle by hue angle into the range of output chromaticities, the mapping of sRGB values to ink surface coverage values is in a first approximation independent of the

specifically chosen white reference. The only differences that may occur concern the details of the mapping of the display chroma intervals into the print chroma intervals (see next section).

Mapping the input sRGB gamut into the print gamut

Gamut mapping aims at bringing all displayable input image colors into the gamut of the metal prints viewed under specular reflection. The display gamut shown as a mesh in Figure 7 must be brought into the print gamut shown as a color volume.

We perform gamut mapping by first performing a linear mapping of the input sRGB gamut lightness range into the target specular print gamut lightness range and then a chroma mapping according to the scheme shown in Fig. 9. This chroma mapping relies on a two-foci mapping approach [24].

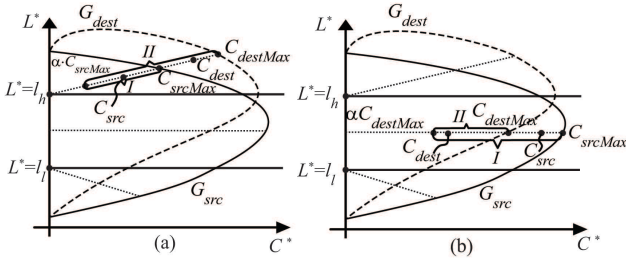

***Figure 9**. Principle of chroma mapping between a lightness adapted source gamut G_{src} and the target print gamut G_{dest} in CIELAB space.*

In the considered case (Figure 7), most parts of the destination gamut are inside the source gamut and little parts of it are outside the source gamut. Figure 9 illustrates the chroma mapping with lower and upper focal points. In the lightness range between the focal points, source chroma values are mapped into destination chroma values by keeping the lightness constant. Outside this lightness range, chroma values are mapped along lines from the focal point to the source chroma value. In case that the source chroma is larger than the destination chroma, chroma reduction occurs by mapping the source chroma interval I into the destination chroma interval II (Figure 9b). In the part of the chroma between C^*=0 and C^*= α $C_{destMax}$ source chroma values are mapped to the same destination chroma values (identity mapping). This avoids the desaturation of low and intermediate chroma values. When the source chroma is smaller than the destination chroma, chroma expansion is performed by mapping source chroma interval I into destination chroma interval II (Figure 9a). In the present implementation, we choose an α value of 0.8 .

At image rendition time, gamut mapped input image colors are separated into individual ink layers by making use of the table specifying the correspondence between desired printed color and ink surface coverages. This table is created once by computing for each CIELAB color within a regular grid the corresponding surface coverages of the inks. Surface coverages of the inks are obtained with the IS-CYNSN model (Section 5) by performing a gradient descent until the desired CIELAB color matches the predicted CIELAB color. The ink separations are then halftoned and printed.

Examples of color prints on metal viewed under specular reflection

In order to show the quality of the produced color prints on metal viewed under specular reflection, we have taken pictures of these prints outdoor, illuminated by a partly cloudy sky, with the camera capturing the center of the color print at an angle of 25° from its normal, from a distance of 36 cm.

We have also taken pictures of the same images printed on paper with the same printer, same halftoning parameters, but with the color prediction model calibrated for paper prints and by mapping input sRGB colors to the paper print gamut. Both the metallic and paper print pictures were acquired under the same exposition and capturing geometry, but, in the case of Figures 10 and 11, with an exposure of 1/320 s for the "metallic" prints and of 1/125 s for the paper prints, at the same aperture of *f*/5.6. The camera is a Canon PowerShot S95 digital camera.

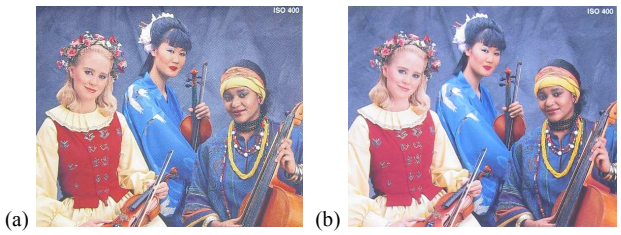

***Figure 10**. (a) Picture of orchestra print on the metal film viewed under specular reflection, taken with an exposure of 1/320 s and (b) picture of orchestra print on paper, taken with an exposure of 1/125 s, under the same illumination and capturing geometry (for details: see the electronic version).*

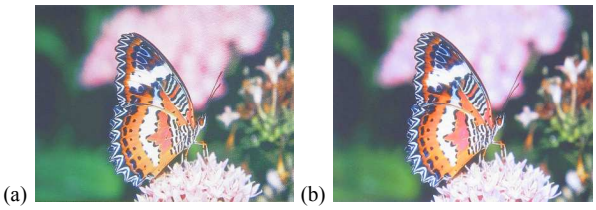

***Figure 11**. (a) Picture of butterfly on the metal film viewed under specular reflection, taken with an exposure of of 1/320 s and (b) picture of butterfly print on paper, taken with an exposure of 1/125 s under the same illumination and capturing geometry.*

The comparison between the metal print and the paper prints shows that the hues of the prints on metal are rendered correctly, compared with the paper prints. The metal prints viewed under specular reflection are at an increased luminance level and their hues are therefore perceived as more colorful. However, due to the acquisition by the camera and the reproduction on paper, this increase in luminance level and the corresponding increase in colorfulness are not visible (Figures 10 and 11).

Under specular observation, the metallic prints have a much higher reflectance and the eye adapts at a considerably higher luminance level. For the color samples printed in the Appendix, under the described illumination and observation conditions, the bare metal film reflects a luminance of 7600 cd/m^2 and the chromatic black sample printed on metal reflects a luminance of 470 cd/m^2. Under the same illumination and observation conditions, the unprinted paper reflects a luminance of 2900 cd/m^2

and the printed chromatic black sample on paper reflects a luminance of 190 cd/m^2.

Conclusions

We presented a full reproduction workflow for printing color images on metallic substrates. This color reproduction workflow relies on the ink spreading enhanced cellular Yule-Nielsen modified spectral Neugebauer model [15]. The model is calibrated with 35 uniform color samples printed on the metal film measured under specular reflection. The calibrated model accounts for the phenomena contributing to the appearance of the metallic colors under specular reflection: specular reflection of light traveling across the inks by the metal film substrate, shadowing effect induced by the ink dots and difference in surface structure between the inked and non-inked metal halftone surface parts. The model calibration is valid only for a given set of inks and substrate, halftoning method and for a given illumination and observation geometry. Under these conditions, the model enables predicting all other printable colors with an average CIELAB ΔE_{94} accuracy of 1.7. These predictions are used to create the metal print gamut. Display sRGB colors are mapped to this print gamut, halftoned and printed.

The resulting printed color images on metal viewed under specular reflection reproduce the hues at a high degree of fidelity. Since the luminance of metallic prints under specular observation is higher than the luminance of paper under the same illuminating conditions, the printed metallic colors appear more colorful.

Metallic prints viewed under specular reflection may become attractive for art and publicity. Their high brightness immediately strikes the observer and transmits the message incorporated into the reproduced picture or artwork.

Despite the fact that we have established a workflow capable of reproducing color images on metallic substrates, many related issues need to be explored. The proposed color reproduction workflow relies on a CIELAB space extension where the reference white is the unprinted metal film under specular reflection. Does such a CIELAB space respect classical CIELAB visual features, such as equal visual distances for equal intervals between samples, at least when varying separately the lightness, chroma or hue values? At present, the model needs to be recalibrated when modifying the specular illumination and observation angle. A future goal would be to establish a model for halftone prints on metal where the illuminating and capturing geometry would be expressed as a freely chosen input parameter. Such a model would also need to account for the illumination and observation angle dependent shadowing effect.

References

[1] J. Morovic, J. Lammens, Color Management, in Colorimetry: Understanding the CIE system, (Ed. J. Schanda), Chapter 7, J. Wiley, 159-206 (2007).

[2] Epson Seiko silver film, metallic PET base, 4.7 mil thickness, 165 gsm.

[3] Fairchild M.D., Color Appearance Models, Addison-Wesley, 2nd Edition (2005).

[4] M. D. Fairchild and P.H. Chen, "Brightness, lightness, and specifying color in high-dynamic-range scenes and images", Proc. SPIE 7867, Image Quality and System Performance VIII, paper 78670O, 14 pages (2011).

[5] N. Moroney, M.D. Fairchild, R.W.G Hunt, C.J. Li, M.R. Luo, T. Newman. "The CIECAM02 Color Appearance Model", in IS&T 10th Color Imaging Conference, 23-27 (2002).

[6] C.J. Li, M.R. Luo, R.W.G Hunt, N. Moroney, M.D. Fairchild, T. Newman. "The performance of CIECAM02", in IS&T 10th Color Imaging Conference, 28-32 (2002).

[7] E. Reinhard, S. Pattanaik, G. Ward, P. Debevec, High dynamic range imaging, acquisition, display and image-based lighting, Morgan Kaufmann (2006). See Section 6.2, pp. 191-218.

[8] E.D. Dalal, K.M. Natale-Hoffman, The Effect of Gloss on Color, Color Research and Application, Vol. 24, No. 5, 369-376 (1999)

[9] Milan Mikula, Michal Ceppan, Karol Vasko, Gloss and Goniocolorimetry of Printed Materials. Color Research and Application, Vol. 28, No. 5, 335-342 (2003).

[10] R.D. Hersch, F. Collaud, P. Emmel, Reproducing color images with embedded metallic patterns, Proc. Siggraph, ACM Trans. on Graphics, Vol. 22, No.3, 427-436 (2003).

[11] W. Matusik, B. Ajdin, J. Gu, J. Lawrence, H. P. A. Lensch, F. Pellacini, S. Rusinkiewicz, Printing Spatially-Varying Reflectance, Proc. Siggraph Asia 2009, in ACM Trans. on Graphics, Vol. 28, no.5, paper 128, 9 pages (2009).

[12] J.A.S. Viggiano, "Modeling the color of multi-colored halftones," Proc. TAGA, vol. 42, 44-62 (1990).

[13] R.Balasubramanian, Optimization of the spectral Neugebauer model for printer characterization, J. Electronic Imaging, Vol. 8, No. 2, 156-166, 1999.

[14] Heuberger, KJ, Jing, ZM, and Persiev S. (1992) Color Transformations and lookup tables, in TAGA/ISCC Proceedings, 863-881.

[15] R. Rossier, R.D. Hersch, Introducing ink spreading within the cellular Yule-Nielsen modified Neugebauer model, IS&T 18th Color Imaging Conference, 295-300 (2010).

[16] L. Simonot, M. Hébert, D. Dupraz, Goniocolorimetry: from measurement to representation in the CIELAB color space, Color Research and Application, Vol. 36, Issue 1, 1-10 (2011).

[17] G.M. Johnson and M.D. Fairchild, Visual psychophysics and color appearance, In Digital Color Imaging Handbook, Ed. Sharma, Chapter 2, 115-171 (2003).

[18] R.W.G. Hunt, M.R. Pointer, A Colour appearance transform for the CIE 1931 Standard Colorimetric Observer, Color Research and Applications, Vol. 10, 165-179 (1985).

[19] R.W.G. Hunt, Light and dark adaptation and the perception of color, J. Opt. Soc. Am. 42, 190-199 (1952).

[20] Stevens, J.C. and Stevens S.S. Brightness functions: effects of adaptation, J. Opt. Soc. Am. 53, 375-385 (1963).

[21] Fairchild M.D., Pirotta E., Predicting the lightness of chromatic object colors using CIELAB, Color Res. Appl. Vol. 16, 385-293 (1991).

[22] G. Sharma, Color fundamentals for digital imaging, in Digital Color Imaging Handbook (G. Sharma Ed.), Chapter 1, CRC Press, 1-114 (2003).

[23] F. Bernardini, J. Mittleman, H. Rushmeier, C. Silva, and G. Taubin, The Ball-Pivoting Algorithm for Surface Reconstruction, IEEE Trans. Visualization and Computer Graphics, vol. 5, no. 4, pp. 349-359 (1999).

[24] J. Morovic, M. R. Luo, The fundamentals of gamut mapping: A survey, J. Imag. Sci. Technol., vol. 45, no. 3, pp. 283–290 (2001).

Appendix

A. Pictures of the 27 samples used for calibrating the IS-YNSN model.

The pictures shown in Figs. 12 and 13 are formed by combinations of 0%, 50% and 100% ink surfaces coverages of cyan, magenta and yellow both for the print on metal and for the print on paper. These two pictures were taken under the same illumination and capturing geometries by the Canon PowerShot S95 camera, under outdoor illumination.

***Figure 12**. Picture of printed uniform samples on the metal film taken at an exposure of 1/250 s, with an aperture of F5.6.*

***Figure 13**. Picture of the corresponding printed uniform samples on paper taken at an exposure of 1/125 s, with an aperture of F5.6.*

B. Effect of scaling down the white reference

Let us recall the formula for calculating the CIELAB values from CIE-XYZ tri-stimulus values, for patches fulfilling the conditions $X/X_w>0.008856$, $Y/Y_w>0.008856$, and $Z/Z_w>0.008856$, where X_w, Y_w, and Z_w express the tri-stimulus values of the reference white [Sharma 2003]:

$$L^* = 116\cdot\left(\frac{Y}{Y_w}\right)^{\frac{1}{3}} - 16\,;\; a^* = 500\cdot\left(\left(\frac{X}{X_w}\right)^{\frac{1}{3}} - \left(\frac{Y}{Y_w}\right)^{\frac{1}{3}}\right);$$
$$b^* = 200\cdot\left(\left(\frac{Y}{Y_w}\right)^{\frac{1}{3}} - \left(\frac{Z}{Z_w}\right)^{\frac{1}{3}}\right) \quad \text{(B1)}$$

In the present case, we have chosen as reference white the CIE-XYZ values X_a, Y_a and Z_a of the blank metal, i.e. $X_w=X_a$, $Y_w=Y_a$, $Z_w=Z_a$. If instead, we would choose as reference white the CIE-XYZ values of the blank metal scaled down by a multiplicative factor $g<1$, we would obtain the following CIELAB values

$$L^* = 116\cdot\left(\frac{Y}{gY_a}\right)^{\frac{1}{3}} - 16 = 116\cdot\left(\frac{1}{g}\right)^{\frac{1}{3}}\left(\frac{Y}{Y_a}\right)^{\frac{1}{3}} - 16$$
$$a^* = 500\cdot\left(\left(\frac{X}{gX_a}\right)^{\frac{1}{3}} - \left(\frac{Y}{gY_a}\right)^{\frac{1}{3}}\right) = 500\cdot\left(\frac{1}{g}\right)^{\frac{1}{3}}\left(\left(\frac{X}{X_a}\right)^{\frac{1}{3}} - \left(\frac{Y}{Y_a}\right)^{\frac{1}{3}}\right) \quad \text{(B2)}$$
$$b^* = 200\cdot\left(\left(\frac{Y}{gY_a}\right)^{\frac{1}{3}} - \left(\frac{Z}{gZ_a}\right)^{\frac{1}{3}}\right) = 200\cdot\left(\frac{1}{g}\right)^{\frac{1}{3}}\left(\left(\frac{Y}{Y_a}\right)^{\frac{1}{3}} - \left(\frac{Z}{Z_a}\right)^{\frac{1}{3}}\right)$$

Formula (B2) show that by taking as white reference the blank metal tri-stimulus values scaled down by a multiplicative factor $g<1$, the corresponding CIELAB values are scaled up by the cube root of the reciprocal of g. Figure 12 gives the L^*, a^* and b^* scaling factors as a function of the multiplicative factor g.

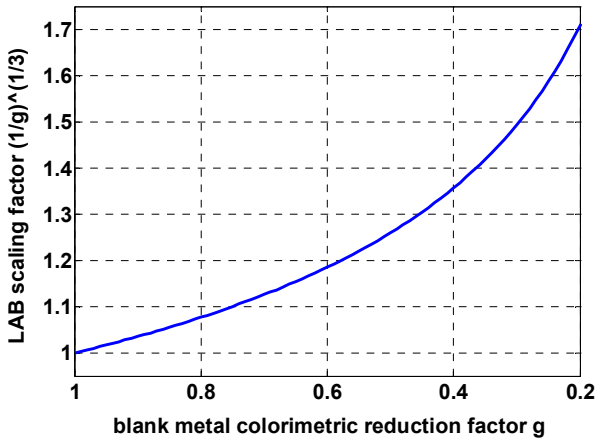

***Figure 14**. L^*, a^*, b^* scaling factor obtained as a function of the scaling factor g applied to scale down the blank metal tri-stimulus values for setting the CIELAB white reference used for the adaptation of the human visual system.*